Image and Vision Computing 28 (2010) 223–230

Contents lists available at ScienceDirect

Image and Vision Computing

journal homepage: www.elsevier.com/locate/imavis

Efficient and robust segmentation of noisy iris images for non-cooperative iris recognition

Tieniu Tan *, Zhaofeng He, Zhenan Sun

Center for Biometrics and Security Research, National Laboratory of Pattern Recognition, Institute of Automation, Chinese Academy of Sciences, P.O. Box 2728, Beijing 100190, PR China

ARTICLE INFO

Article history:
Received 29 December 2008
Received in revised form 5 May 2009
Accepted 14 May 2009

Keywords:
Coarse iris localization
Eyelid and eyelash detection
Iris segmentation
Non-cooperative iris recognition

ABSTRACT

This paper describes the winning algorithm we submitted to the recent NICE.I iris recognition contest. Efficient and robust segmentation of noisy iris images is one of the bottlenecks for non-cooperative iris recognition. To address this problem, a novel iris segmentation algorithm is proposed in this paper. After reflection removal, a clustering based coarse iris localization scheme is first performed to extract a rough position of the iris, as well as to identify non-iris regions such as eyelashes and eyebrows. A novel integrodifferential constellation is then constructed for the localization of pupillary and limbic boundaries, which not only accelerates the traditional integrodifferential operator but also enhances its global convergence. After that, a curvature model and a prediction model are learned to deal with eyelids and eyelashes, respectively. Extensive experiments on the challenging UBIRIS iris image databases demonstrate that encouraging accuracy is achieved by the proposed algorithm which is ranked the best performing algorithm in the recent open contest on iris recognition (the Noisy Iris Challenge Evaluation, NICE.I).

1. Introduction

Recently, non-cooperative iris recognition has attracted much attention since it greatly extends the applicability of iris recognition [1–3]. In non-cooperative iris recognition, the user has little or even no active participation in the image capture process [4]. As a result, the iris images are often captured with more noisy artifacts, such as blur, reflections, occlusions, oblique view-angles, etc., making non-cooperative iris recognition challenging.

Since 1998, we at CASIA[1] have devoted significant efforts towards iris recognition and most recently non-cooperative iris recognition. We have addressed many issues in (non-cooperative) iris recognition such as image quality evaluation [5], iris segmentation [6], feature extraction and classification [7–9], coarse iris classification [10], iris spoof detection [11] and iris image synthesis [12]. Regarding the hardware design, particular attention has also been paid on non-cooperative iris recognition. One undergoing project at CASIA addresses non-cooperative iris recognition in several interesting scenarios such as on-the-move and at-a-distance [13].

During the development, we realized that one of the bottlenecks for a working non-cooperative iris recognition system is efficient and effective segmentation of noisy iris images. Iris segmentation is an essential module in iris recognition because it defines the valid region used for feature extraction, and therefore is directly related to the recognition accuracy [6]. Thus, a segmentation method that can cope with various types of noise is important and desirable especially for non-cooperative iris recognition.

Many researchers have contributed much in iris segmentation, and encouraging performance has been achieved [1,3,14,15]. In this paper, we present a novel iris segmentation method, aiming at noisy iris images in non-cooperative or less-cooperative environments. As illustrated in Fig. 1, it incorporates four key modules, namely coarse iris localization based on clustering, localization of pupillary and limbic boundaries, eyelid localization and eyelash/shadow detection.

The remainder of this paper is organized as follows. In Sections 2–5, the technical details of the four modules of the proposed algorithm are presented step by step. Extensive experiments are described and discussed in Section 6 prior to the conclusions in Section 7.

In passing, it should be pointed out that only the red component of the color iris image is utilized because the iris presents more sensitivity to infrared wavelength [13], and therefore the red component should convey the most useful information for iris segmentation.

2. Coarse iris localization based on clustering

It has been reported that most mis-localizations occur on non-iris regions due to the high local contrast (e.g. on eyelashes, eyebrow or glass frame). A straightforward idea to avoid such mis-localizations is therefore to exclude the non-iris regions at

* Corresponding author. Tel.: +86 1062632265.
E-mail addresses: tnt@nlpr.ia.ac.cn (T. Tan), zfhe@nlpr.ia.ac.cn (Z. He), znsun@nlpr.ia.ac.cn (Z. Sun).

[1] Institute of Automation, Chinese Academy of Sciences (CASIA).

0262-8856/$ - see front matter © 2009 Elsevier B.V. All rights reserved.
doi:10.1016/j.imavis.2009.05.008

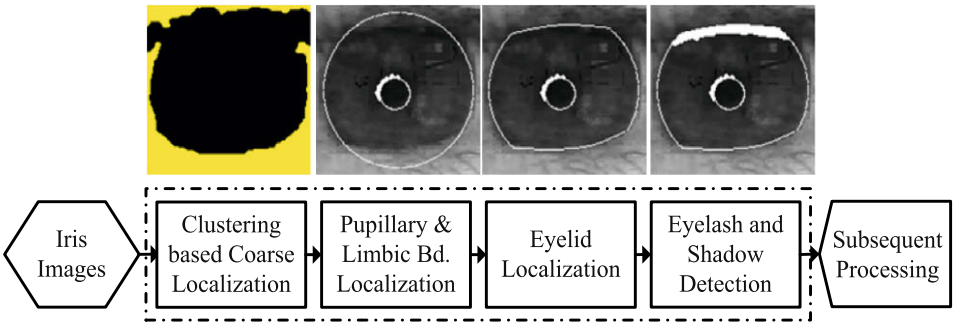

Fig. 1. The flowchart of the proposed iris segmentation method.

the coarse iris localization step. Obviously, if we can cluster and label the iris image as candidate iris region, skin region and eyebrow region at the coarse iris localization step (see Fig. 2(e)), we can easily avoid such mis-localizations by exclusively performing fine iris localization on the candidate iris region (rather than on eyelashes, eyebrow, etc.). The problem then becomes how to cluster the whole iris image into different parts, and label each part as candidate iris region or non-iris regions. In this work, an eight-neighbor connection based clustering method is proposed to address this problem.

However, direct clustering on original iris images tends to fail due to the structural interruptions of specular reflections in the images. To alleviate this problem, a novel reflection detection and removal scheme has been proposed based on adaptive thresholding followed by bi-linear interpolation. Due to the page limitation, we refer the readers to our earlier work [6] for more details. One example of reflection removal is shown in Fig. 2(b). We can see that most of the reflections have been correctly filled, which paves the way for the following eight-neighbor connection based clustering.

2.1. Eight neighbor connection based clustering

The objective of the clustering method here is to cluster the whole iris image into different parts according to their structure. It works as follows:

2.1.1. Initialization

A common property of iris images is that the intensity of the iris region is relatively lower than that of the skin region. Accordingly, we assign the top p_1 brightest points as the skin region and the top p_2 darkest points as the candidate iris regions. Clearly, the larger the p_1 and p_2, the faster the clustering will converge. However, p_1 and p_2 with too large values will induce confusion between the skin region and the iris region. In principle, p_1 (p_2) should be set so that a fraction of the skin (iris) region will be initialized. Our experiments show that $p_1 = 30\%$ and $p_2 = 20\%$ are reasonable for the NICE iris image database [4]. Note that the eyelash, eyebrow regions can also be mistaken as candidate iris regions at this stage since their intensities are relatively low as well. Fig. 2(c) illustrates clustering initialization, where the yellow region R_2 denotes candidate skin region, while the black R_1 and green R_3 regions denote the candidate iris regions.

2.1.2. Clustering un-clustered points

The next step is to cluster the un-clustered points into different regions, which is iteratively done as follows:

Step-1: Calculate the average gray level (g_R) and standard deviation (d_R) of each candidate region R.
Step-2.1: Randomly choose one candidate region R, and calculate the distance of each un-clustered point to this region via the following point-to-region distance:

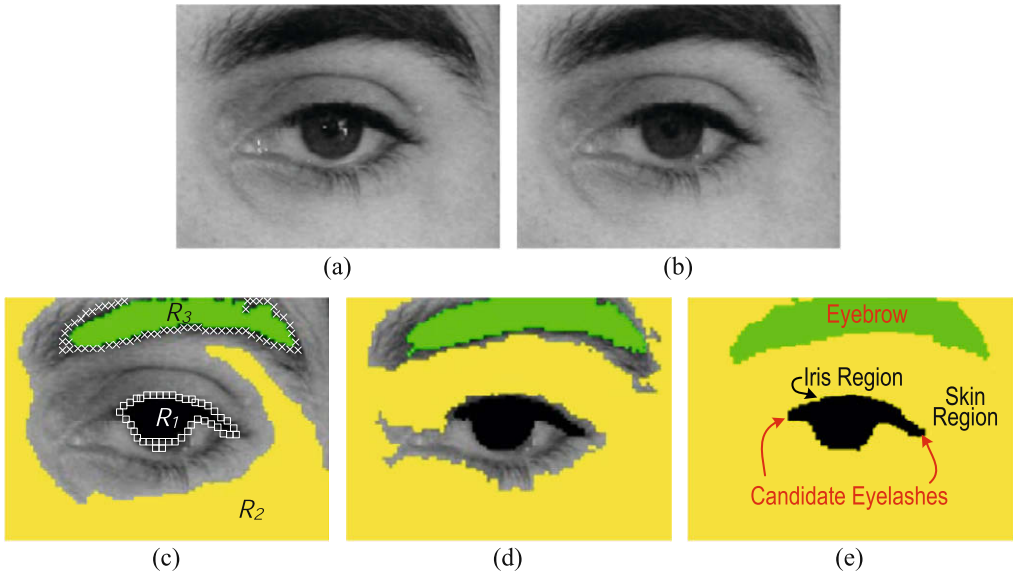

Fig. 2. Illustration of reflection removal and eight-neighbor connection based clustering. (a) The original iris image. (b) The iris image after specular reflection removal. (c) Clustering initialization. (d) Clustering result after the first (*Step-1* and *Step-2*) iteration. (e) Semantic labeling. After reflection removal, the original iris image is clustered into different parts. And the semantic priors enable a coarse identification of each part.

$$D(P,R) = \frac{|g_P - g_R|}{d_R} \quad (1)$$

where g_P is the intensity of the un-clustered point.

Step-2.2: Evaluate whether the un-clustered points can be clustered into this candidate region. Point P is clustered into region R if it satisfies: (1) $D(P,R)$ is less than a threshold T_{P2R} (=2.5 in this work). (2) There exists a valid eight-neighbor connection path that connects P to R. Take region R_1 (labeled as black) in Fig. 2(c) as an example. Both the '×' and '□' points satisfy criterion 1 (i.e. $D(P,R_1) < T_{P2R}$). However, the '×' points do not meet Criterion 2 because they cannot be eight-neighbor connected to region R_1 due to the interruption of un-clustered points. Therefore, they cannot be clustered into region R_1, whereas the '□' points can.

Step-2.3: Repeat *Step-2.1* and *Step-2.2* for each candidate region. Fig. 2(d) shows the clustering result after *Steps 2.1–2.3*, where most un-clustered points have been clustered into separate candidate regions.

Step-3: Repeat *Step-1* and *Step-2* until all the un-clustered points are clustered into some region, see Fig. 2(e).

From the descriptions, we can see that the proposed clustering method is essentially a region growing algorithm via the point-to-region distance and eight-neighbor connection.

2.2. Semantic refinements

An even challenging problem after clustering is to further identify these clustered regions as candidate iris region or non-iris regions for the purpose of coarse iris localization. Although the skin region can be easily identified via its intensity, other regions (e.g. eyelashes, eyebrow, hair and glass frames) remain difficult to identify. This problem is tackled with the assistance of several semantic priors, such as:

1. A genuine candidate iris region usually has a '–○–' like shape whose center is much thicker than its left and right ends, as shown in Fig. 2(e). This is because the center corresponds to the iris, whereas the left and right ends are due to eyelashes or shadows of upper eyelid.
2. The eyebrow region is usually a horizontal dark stripe above the candidate iris region, see Fig. 2(e).
3. A glass frame usually has a dark and approximately rectangle-like shape as shown in Fig. 6(b).

With these priors, semantic labeling can be achieved as shown in Fig. 2(e). A coarse estimation of the iris position is therefore obtained. However, the problem is how to let the computer understand these semantic priors. In this work, shape, intensity and position of each clustered region are adopted to extract such semantic information. While the intensity and position are self-explained, shape is hard to represent. In our original algorithm (submitted to NICE.I), the shape of each clustered region is represented via its height-to-width ratio, the height of each column, etc. More recently, we found that shape-moment or Fourier descriptor should be a more effective measure [16].

3. Pupillary and limbic boundary localization

Region clustering and semantic refinements enable a coarse estimation of the iris position. However, we have to further finely localize the pupillary and limbic boundaries of the iris for the purpose of iris recognition. In this work, the pupillary and limbic boundaries of the iris are modeled as two non-concentric circles, and the well-known integrodifferential (ItgDiff for short) operator is adopted for its robustness to various noisy artifacts [14]:

$$\max_{(r,x_0,y_0)} \left| G_\sigma(r) * \frac{\partial}{\partial r} \oint_{r,x_0,y_0} \frac{I(x,y)}{2\pi r} ds \right| \quad (2)$$

However, the original ItgDiff operator suffers greatly from local optima and heavy computation (due to exhaustive search for maximizing Eq. (2)). We propose a novel ItgDiff constellation to tackle both problems.

3.1. ItgDiff-ring

Inspired by gradient descent, a straightforward solution for speeding up the ItgDiff operator is to iteratively find the optimal (shortest) path to maximize Eq. (2). However, this is not trivial because Eq. (2) does not have an analytic expression. That is, we cannot directly get the optimal transition direction via differentiating Eq. (2). Instead, we construct a so-called ItgDiff ring to calculate the search direction we should step forward.

An example of the ItgDiff ring is shown in Fig. 3(a). The basic idea is this: suppose P_0 is the current search point, we calculate the ItgDiff operator on its eight-neighbor points, and step forward towards the one that obtains the highest ItgDiff score. Consequently, we can search along a path that is always locally optimal.

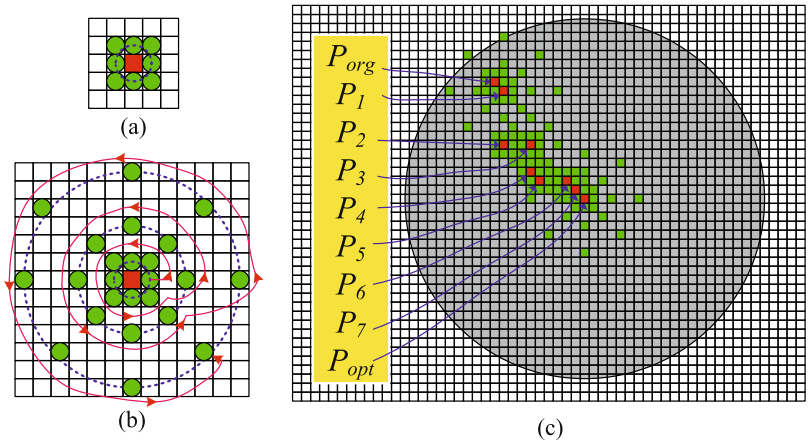

Fig. 3. Illustration of (a) ItgDiff ring, (b) ItgDiff constellation and (c) the search procedure. In (b), the arrowed red line indicates the search index of each validation point. In (c), the green and red points show the actually evaluated points during ItgDiff search, between which the red ones show the optimal transition path. We can see that only a fraction of the candidate (gray) points are evaluated instead of an exhaustive ItgDiff search. Also note the usefulness of the "stop at once" strategy in accelerating the computation.

Moreover, we use an aggressive "stop at once" strategy. That is, once one neighboring pixel's ItgDiff score is higher than the current search point, we stop and turn to this point. Clearly, the "stop at once" strategy raises the risk of choosing a sub-optimal path; however, we found this strategy to be very effective in finding a transition path very close to the optimal one while saving much computation time, especially with the assistance of the following validation constellation.

3.2. ItgDiff-constellation

One drawback of this simple eight-neighbor ItgDiff ring is that it will almost always be trapped in local optima: it is relatively easy to find a point whose ItgDiff score is larger than its eight-neighbors'. To avoid local optima, we add several ItgDiff rings with increasing radii to construct an ItgDiff constellation, see Fig. 3(b). The inspiration is that while it is highly possible to find an eight-neighbor optima, it becomes harder and harder when the ItgDiff constellation grows larger.

Clearly, the larger the ItgDiff constellation, the more likely the ItgDiff search procedure converges on the global optimal. However, larger constellation means more computation. In this work, we adopt three ItgDiff rings with a radius of 1, 3 and 6 whose validation points are scatted as shown in Fig. 3(b).

Fig. 3(c) shows the search procedure, where P_{org} is the starting search point (e.g. obtained via coarse iris localization). Then, we start the search (validation) procedure according to the red line in Fig. 3(b). Suppose ItgDiff(P_1) is larger than ItgDiff(P_{org}), then the current search point is updated to P_1 according to the "stop at once" strategy. The above procedure is repeated and finally converged on the point whose ItgDiff score is larger than all its ItgDiff-Constellation points. From Fig. 3(c) we can see that only a fraction of the candidate (gray) points are evaluated instead of an exhaustive ItgDiff search, which greatly accelerates the computation while guaranteeing a global optimum.

The introduction of the ItgDiff constellation during ItgDiff search changes the problem as we go along. That is, transition direction that seems optimal earlier may prove to be suboptimal on larger ItgDiff ring. This gives justification to not spending too much effort trying to find the optimal transition direction over the whole constellation but just a moderately good one according to the "stop at once" strategy.

3.3. Boundary refinement

In non-cooperative iris recognition, the pupillary and limbic boundaries tend to be non-circular or be occluded. It is therefore necessary to further refine the results by eliminating localization inaccuracies due to the simple circle model we used. However, traditional edge map based methods (e.g. Fourier series expansion [2], cubic smoothing spline [6]) usually fail because of the difficulty in detecting sufficient valid edge points (on the ambiguous boundary). Instead, we try to detect and eliminate the localization inaccuracies via intensity statistics [2]. In detail, the intensity distributions of two consecutive annular rings (e.g. $[R_p - D, R_p]$ and $[R_p, R_p + D]$) are calculated. The intersection point of the two histograms is taken as an adaptive threshold to assign the brightest points in $\mathrm{Hist}_{[R_p-D,R_p]}$ as iris and the darkest points in $\mathrm{Hist}_{[R_p,R_p+D]}$ as pupil.

A similar method is applied to refine the limbic boundary. And morphological operators are used to consider and evaluate the spatial connection of the refined points [6].

4. Eyelid localization

As pointed out in [6], two issues make accurate eyelid localization challenging: one is the eyelash occlusion, and the other is the shape irregularity of eyelids. In our earlier work [17], a horizontal *1-D* rank filter and a eyelid curvature model have been proposed to tackle both problems, respectively.

Based on the observation that the eyelashes are mostly vertical, thin and dark (see Fig. 4(a)), we adopted a *1-D* horizontal rank filter (with length $L = 7$ and rank $p = 2$ [17]) for eyelash removal. Fig. 4(b) shows the result of performing the *1-D* rank filter on Fig. 4(a). We can see that most of the eyelashes are weakened or even eliminated depending on their width.

Meanwhile, horizontal rank filter provides a clearer vertical boundary, and therefore facilitates eyelid edge detection. Edge points are then detected with the Canny operator along vertical direction. To avoid noisy edge points, only one edge point is reserved in each column as shown in Fig. 4(c). As a consequence, a raw edge map of the eyelid E_{raw} is obtained.

However, E_{raw} often contains some noisy points due to various noisy artifacts as shown in Fig. 4(c). Usually, there is no highly reliable method to eliminate such noise due to the shape irregularity of eyelids. To tackle this problem, a so-called eyelid curvature model is statistically established (by manually labeling and averaging the eyelid curves of iris images in the training database), see Fig. 4(d). The insight is that although the shapes of eyelids vary considerably from image to image, they possess a common arc structure. For example, the eyelid in Fig. 4(f) can be decomposed into an up-right arc and a straight line as shown in Fig. 4(e). Clearly, if we can accurately estimate this arc structure and subtract it from the raw eyelid E_{raw}, the result should resemble a straight line, which can be easily fitted with, for example, simple line Hough transforms. Note that the line Hough transforms here provide cues for noise elimination. That is, only the points that are in accordance with the best fitting line are reserved as genuine eyelid points, while other points that are distant from the best fitting line are eliminated as noise.

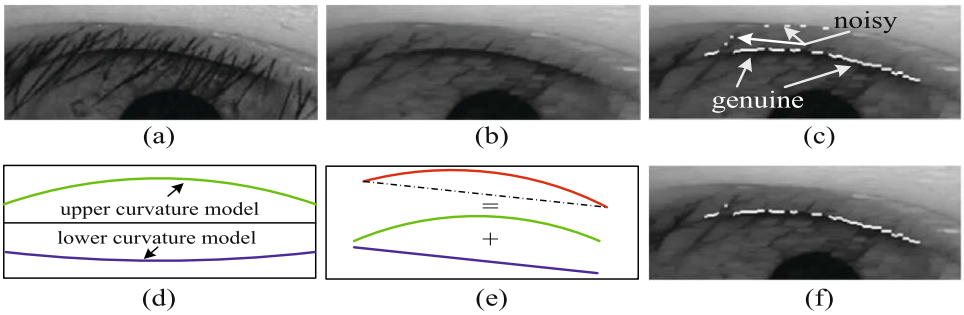

Fig. 4. An illustration of eyelid localization. (a) Original iris image. (b) Eyelashes removal via the *1-D* horizontal rank filter. (c) The raw eyelid edge map E_{raw}. (d) The learned eyelid curvature models. (e) The decomposition of the eyelid in (f). (f) The genuine eyelid edge map after noise elimination with the curvature model.

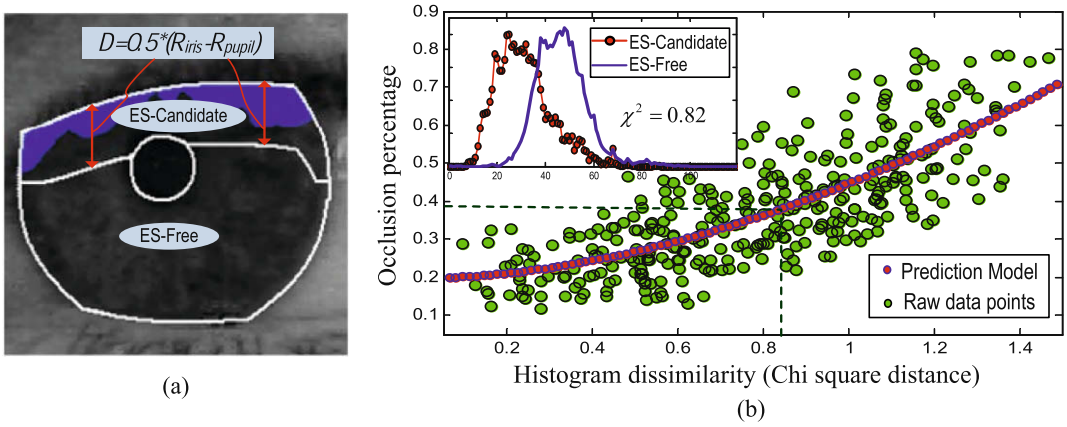

Fig. 5. Eyelash and shadow detection via the learned prediction model. (a) Adaptive iris division into ES_{free} and $ES_{candidate}$. (b) The prediction model for eyelash and shadow detection. This prediction model provides a coarse estimation of the appropriate threshold for ES detection.

Once these noisy edge points are eliminated from E_{raw} (see Fig. 4(f)), a more refined eyelid can be obtained via parabolic curve fitting. The shape irregularity is therefore effectively addressed by the eyelid curvature model. Here, the eyelid curvature model is useful because "it improves the localization accuracy than direct parabolic curve fitting on E_{raw} by eliminating noisy edge points" [17].

A similar approach is used to locate the lower eyelid, with another lower eyelid curvature model shown in Fig. 4(d). More details about this eyelid localization method can be found in [17].

5. Eyelash and shadow detection

Eyelashes and shadows (ES) are another source of occlusions that challenge iris segmentation. In [6], we have proposed a novel method for ES detection, whose basic idea is to extract an appropriate threshold for ES detection via a statistically established prediction model.

The most visible property of ES is that they are generally darker than their backgrounds (eyelids or iris), and a straightforward detection strategy is therefore thresholding. However, usually it is hard to get a proper threshold due to the variation of the intensity and amount of ES between individual iris images, especially on noisy ones. In [2], Daugman pointed out that the intensity distributions of different iris regions are different and can be utilized for determining a proper threshold for ES detection. For example, in Fig. 5(a), the candidate iris region is divided into two parts (ES_{free} and $ES_{candidate}$, respectively), and the corresponding intensity histograms of both regions are shown on the top-left corner of Fig. 5(b). Clearly, the histogram of $ES_{candidate}$ is quite different from that of ES_{free} due to the occlusion of eyelashes and shadows. Furthermore, it is straightforward to assume that the more occlusions, the larger difference between them. Conversely, we can predict the amount of the ES occlusions according to the level of difference between the two histograms.

To validate the above assumption, we calculate the relationships between the amount of ES occlusions and the difference between histograms of ES_{free} and $ES_{candidate}$ on 400 iris images from the NICE.I Training database. The results are shown in Fig. 5(b), where x-axis is the histogram dissimilarity (measured by χ^2 distance[2]), y-axis denotes the percentage of occlusions in the image (manually obtained), and the green circles '$\circ$' denote the relations of each specific iris image. Fig. 5(b) experimentally confirms our assumption: the larger difference between the intensity histograms of ES_{free} and $ES_{candidate}$, the more occlusions in the iris image.

In order to predict the amount of ES occlusion according to the difference between the two intensity histograms, a prediction model is learned by fitting these raw data points (the '$\circ$'s) with a cubic polynomial curve, shown in red in Fig. 5(b). With the assistance of this prediction model, we can get an appropriate threshold for ES detection. For example, if the χ^2 distance of the histograms of ES_{free} and $ES_{candidate}$ is 0.82, we can say that the amount of the ES occlusion is about 39%. Accordingly, we set the detection threshold to the intensity up to which the sum of the histogram of $ES_{candidate}$ is above 39%. Thus, an adaptive ES detection threshold is obtained, which results in an impressive detection result as shown in Fig. 5(a). We refer the readers to [6] for more details of the prediction model as well as some post-refinement strategies.

6. Experiments

In this section, experiments are carried out on the UBIRIS iris image databases [4,18] to evaluate the effectiveness of the proposed methods.

6.1. The UBIRIS iris image databases

The UBIRIS iris image databases consist of three subsets, namely UBIRIS v1.0 Session 1, Session 2 and UBIRIS v2.0 Train, with about 2377 images in total. Many realistic noise factors (e.g. reflections, luminosity, occlusions, blur, oblique view angle and non-iris image) were introduced especially in UBIRIS v2.0 Train, simulating non-cooperative imaging environment (e.g. acquired covertly or from a distance). Therefore, the UBIRIS iris image databases are suitable for iris segmentation evaluation. Moreover, the binary ground truth for segmentation of UBIRIS v2.0 Train has also been manually labeled and provided by the NICE.I Organizing Committee [4], which enables a quantitative evaluation of the segmentation accuracy. Some typical noisy iris images from NICE.I Train are illustrated in Figs. 6 and 7. These images are obviously challenging for iris segmentation.

6.2. Accuracy of coarse iris localization

In this subsection, we evaluate the accuracy of clustering based coarse iris localization. Here, the accuracy is obtained by visual inspection. We consider coarse localization correct when one and only one candidate iris region covering the whole iris is obtained on iris images, or no candidate on non-iris images. Based on this accuracy measurement, the results on different databases are

[2] The χ^2 distance between two considered histograms h_1 and h_2 is calculated by $\chi^2 = \sum_i (h_{1i} - h_{2i})^2/(h_{1i} + h_{2i})$.

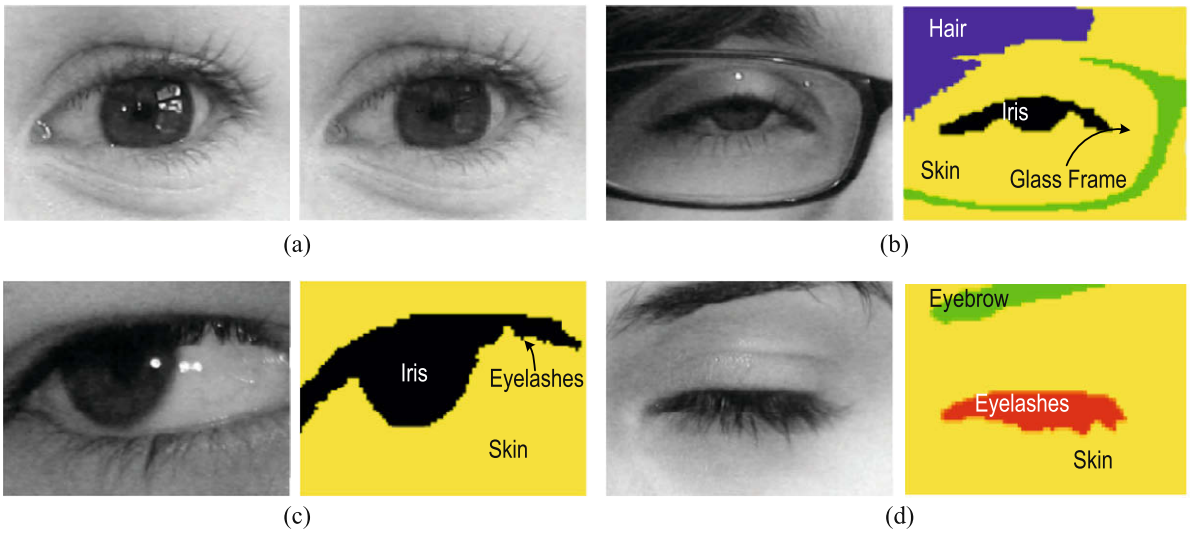

Fig. 6. Illustrations of (a) specular reflection removal and (b)–(d): clustering based coarse iris localization.

shown in Table 1. In addition, examples of coarse iris localization results are shown in Fig. 6.

From Table 1 and Fig. 6 we can see that the clustering based coarse iris localization scheme is capable of identifying the candidate iris region and excluding non-iris regions (e.g. eyebrow, glass frame and eyelashes). However, it must be pointed out that effective reflection removal is a necessity because it alleviates the structural interruptions of reflections, and paves the way for clustering, see Fig. 6(a). Moreover, one must note that the clustering method can only provide a raw clustering result by itself. The most important issue in coarse iris localization (namely the identification of the genuine iris region) is achieved via the semantic refinement scheme described in Section 2.2. This shows the importance and usefulness of the semantic priors on iris localization, especially on non-cooperative iris image localization. Therefore, more complicated semantic prior extraction method should be encouraged in the future.

More interestingly, Table 1 shows that the performance degradation from UBIRIS v1.0 to UBIRIS v2.0 Train is not much for clustering based coarse iris localization, which indicates its robustness to various noise in non-cooperative environments.

6.3. Convergence of the ItgDiff constellation

In this subsection, we test the convergence ability and the efficiency of the ItgDiff constellation. Clearly, the larger the constellation, the more likely the search procedure globally converges. The relationship between the size of the ItgDiff constellation and the convergence ability is shown in Table 2. We can see that the convergence ability greatly increases with the ItgDiff constellation growing larger. Almost 100% convergence on the global optimum can be expected when we use an ItgDiff constellation with three ItgDiff rings and 24 validation points, which is also the setting of this work.

Another important role of the ItgDiff constellation is to accelerate the computation of the original ItgDiff operator. Traditionally, we have to exhaustively evaluate all the points of a candidate region (e.g. the gray points in Fig. 3(c)). However, under the framework of the ItgDiff constellation, only a fraction of the points need to be evaluated. Accordingly, the ratio of the actually evaluated points to the total candidates can be an indicator of the efficiency of the ItgDiff constellation. The results on UBIRIS iris image databases show that only about 23% points are actually evaluated on average under the ItgDiff constellation framework, which means it should be (4.3 = 1/0.23) times faster than the original integrodifferential operator.

6.4. Accuracy illustration and discussions

In this subsection, we quantitatively evaluate the segmentation accuracy and provide some discussions. According to the NICE.I evaluation protocol [4], the segmentation error E on image I is calculated by the proportion of disagreeing pixels (through the logical XOR operator) between O and C:

$$E = \frac{1}{c \times r} \sum_{c'} \sum_{r'} O(c', r') \otimes C(r', c') \tag{3}$$

where O is the binary segmentation result by our algorithm, and C is the corresponding binary ground truth image.

Based on the above evaluation protocol, the segmentation error of the proposed method on NICE.I Train and Test iris image databases are 1.29% and 1.31%, respectively, which is rather promising. Several successful iris localizations (in the presence of eyelids, eyelashes, specular reflections, oblique view angle, glass frame, non-iris image, etc.) are illustrated in Fig. 7(a)–(h), which clearly demonstrate the accuracy and robustness of our methods to typical iris noise in non-cooperative applications.

In our opinion, the main reasons for the promising results are as follows: (1) The reflection removal scheme paves the way for the post-processing. (2) Region clustering and semantic refinements enable identification of the genuine iris region, which significantly reduces the possibility of mis-localizations on non-iris regions. (3) The novel ItgDiff constellation guarantees a globally optimal convergence while accelerating the computation. (4) The eyelid curvature model and the ES prediction model are well tuned to NICE.I images for eyelid, eyelash and shadow localization.

For comparison purpose, we also tried to localize the pupillary and limbic boundaries via edge map based methods (e.g. the Hough transforms [15] and the pulling and pushing method [6]) except for the ItgDiff operator. However, experimental results showed that both edge map based methods degraded greatly when encountered with the noisy iris images in NICE.I. That is perhaps because the NICE.I images contain so much noise that edge map based methods tend to fail due to the lack of valid edge points. Therefore, more efficient edge detection schemes are desirable for these edge map based methods on noisy iris images.

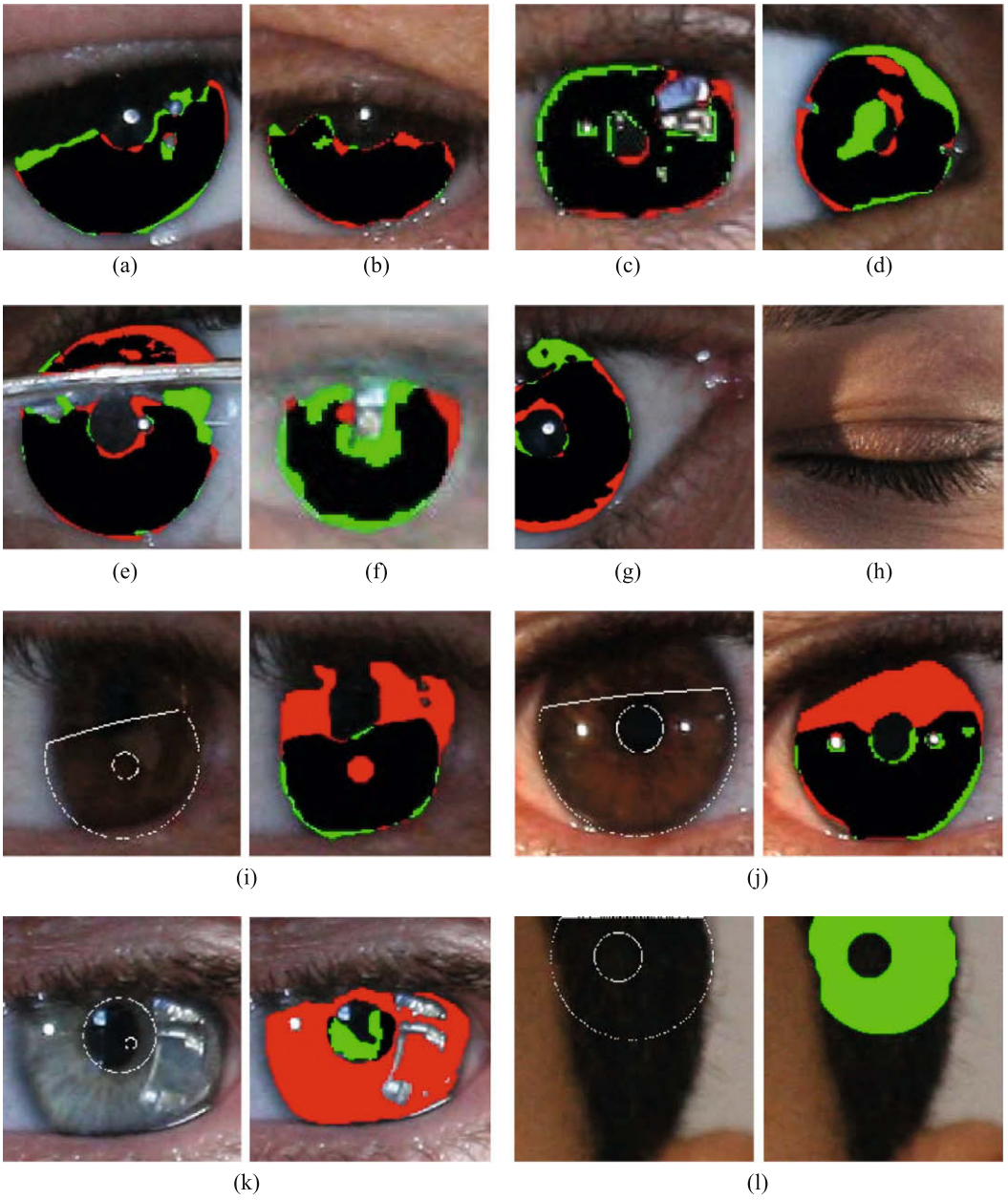

Fig. 7. Illustrations of successful segmentations ((a)–(h)) and inaccurate segmentations ((i)–(l)), where the green points denote false accept points (i.e. points labeled as non-iris by the ground truth but iris by our method), the red points denote false reject points (i.e. points labeled as iris by the ground truth but non-iris by our method), and the black points are labeled as iris by both.

Table 1
The accuracy of clustering based coarse iris localization.

Database	UBIRIS v.1 Session 1	UBIRIS v.1 Session 2	UBIRIS v.2 Train
Accuracy (%)	100	99.4	99.2

Table 2
Convergence ability of the ItgDiff constellation.

Number of rings vs. points	UBIRIS v.1 Session 1	UBIRIS v.1 Session 2	UBIRIS v.2 Train
$1 \leftrightarrow 8$ (%)	24.6	18.4	16.2
$2 \leftrightarrow 16$ (%)	60.1	54.3	50.4
$3 \leftrightarrow 24$ (%)	100	99.8	99.6

Although encouraging performance has been achieved, there are still some iris images that are segmented not as accurately as expected as shown in Fig. 7(i)–(l). In Fig. 7(i), the inaccurate segmentation is due to the non-circular geometry of the iris, and in Fig. 7(j), it is due to incorrect eyelid localization. Accordingly, more refined boundaries localization schemes should be encouraged to deal with such problems. In Fig. 7(k), the mis-localization is because of the clustering module mistaking the bright iris as skin. In Fig. 7(l), although the hair region has been correctly clustered, the semantic refinement scheme failed to identify and exclude the hair. Thus, more efficient semantic prior extraction scheme should also be encouraged in the future work.

From the above description, we can see that noisy iris image segmentation still remains an open problem, which deserves more efforts.

7. Conclusions

In this paper, we have presented an efficient and robust algorithm for noisy iris image segmentation in the context of non-cooperative and less-cooperative iris recognition and in response to the NICE.I iris recognition contest. The main contributions are summarized as follows. Firstly, a novel region growing scheme (namely eight-neighbor connection based clustering) is proposed to cluster the whole iris image into different parts. The genuine iris region is then extracted with the assistance of several semantic priors, and the non-iris regions (e.g. eyelashes, eyebrow, glass frame, hair, etc.) are identified and excluded as well, which greatly reduces the possibility of mis-localizations on non-iris regions. Secondly, an integrodifferential constellation is introduced to accelerate the traditional integrodifferential operator, and meanwhile, enhance its global convergence ability for pupillary and limbic boundary localization. Thirdly, a *1-D* horizontal rank filter and an eyelid curvature model are adopted to tackle the eyelashes and shape irregularity, respectively, during eyelid localization. Finally, the eyelash and shadow occlusions are detected via a learned prediction model based on intensity statistics between different iris regions.

Extensive experiments on the challenging UBIRIS iris image databases have shown that the proposed method achieves state-of-the-art iris segmentation accuracy, and therefore can be well adapted for non-cooperative iris recognition.

Acknowledgments

This work is supported by research grants from the National Basic Research Program (Grant No. 2004CB318110), the Natural Science Foundation of China (Grant No. 60736018), the National Hi-Tech Research and Development Program of China (2006AA01Z193 and 2007AA01Z162).

References

[1] K.W. Bowyer, K. Hollingsworth, P.J. Flynn, Image understanding for iris biometrics: a survey, Computer Vision Image Understanding 110 (2) (2008) 281–307.

[2] J. Daugman, New methods in iris recognition, IEEE Transactions on System, Man, and Cybernetics–Part B: Cybernetics 37 (5) (2007) 1167–1175.

[3] Hugo Proença, L.A. Alexandre, Iris segmentation methodology for non-cooperative recognition, IEEE Proceedings of the Vision, Image and Signal Processing 153 (2) (2006) 199–205.

[4] Hugo Proença, L.A. Alexandre, The NICE.I: noisy iris challenge evaluation – part I, in: Proceedings of the of First International Conference on Biometrics: Theory, Applications, and Systems, 2007, pp. 1–4.

[5] Zhuoshi Wei, Tieniu Tan, Zhenan Sun, Jiali Cui, Robust and fast assessment of iris image quality, in: Proceedings of the of International Conference o, Biometrics (ICB06), Hong Kong, 2006, pp. 464–471.

[6] Zhaofeng He, Tieniu Tan, Zhenan Sun, X.C. Qiu, Towards accurate and fast iris segmentation for iris biometrics, IEEE Transactions on Pattern Analysis and Machine Intelligence (2009).

[7] Li Ma, Tieniu Tan, Yunhong Wang, Dexin Zhang, Personal identification based on iris texture analysis, IEEE Transactions on Pattern Analysis and Machine Intelligence 25 (12) (2003) 1519–1533.

[8] Zhenan Sun, Tieniu Tan, Ordinal measures for iris recognition, IEEE Transactions on Pattern Analysis and Machine Intelligence (2009).

[9] Zhaofeng He, Tieniu Tan, Zhenan Sun, X.C. Qiu, Boosting ordinal features for accurate and fast iris recognition, in: Proceedings of the IEEE Conference on Computer Vision and Pattern Recognition (CVPR'08), 2008.

[10] Xianchao Qiu, Zhenan Sun, Tieniu Tan, Coarse iris classification by learned visual dictionary, in: Proceedings of the of Second International Conference on Biometrics, Seoul, 2007, pp. 770–779.

[11] Zhaofeng He, Tieniu Tan, Zhenan Sun, Encient iris spoof detection via boosted local binary patterns, in: Proceedings of the of International Conference on Biometrics, 2009, LNCS 5558, pp. 1087–1097.

[12] Zhuoshi Wei, Tieniu Tan, Zhenan Sun, Synthesis of large realistic iris databases using patch-based sampling, in: Proceedings of the International Conference on Pattern Recognition (ICPR08), Tampa, 2008.

[13] Wenbo Dong, Zhenan Sun, Tieniu Tan, Xianchao Qiu, Self-adaptive iris image acquisition system, in: Proceedings of the SPIE, Biometric Technology for Human Identification, vol. 6944, Orlando, FL, 2008, pp. 6–14.

[14] J. Daugman, How iris recognition works?, IEEE Transactions on Circuits and Systems for Video Technology 14 (1) (2004) 21–30

[15] R. Wildes, Iris recognition: an emerging biometric technology, Proceedings of the IEEE 85 (1997) 1348–1363.

[16] Sven Loncaric, A survey of shape analysis techniques, Pattern Recognition 31 (1998) 983–1001.

[17] Zhaofeng He, Tieniu Tan, Zhenan Sun, X.C. Qiu, Robust eyelid, eyelash and shadow localization for iris recognition, in: Proceedings of the International Conference on Image Processing, San Diego, October 2008, pp. 265–268.

[18] Hugo Proença, L.A. Alexandre, Ubiris: a noisy iris image database, in: Lecturer Notes in Computer Science, vol. 3617, 2005, pp. 970–977. Available from: <http://iris.di.ubi.pt>.